Atmos. Chem. Phys. Discuss., 9, 3871–3920, 2009
www.atmos-chem-phys-discuss.net/9/3871/2009/

Atmospheric Chemistry and Physics Discussions

This discussion paper is/has been under review for the journal *Atmospheric Chemistry and Physics (ACP)*. Please refer to the corresponding final paper in *ACP* if available.

Reinterpreting aircraft measurements in anisotropic scaling turbulence

S. Lovejoy[1], A. F. Tuck[2], D. Schertzer[3,4], and S. J. Hovde[2]

[1]Physics, McGill University, 3600 University st., Montreal, Que. H3A 2T8, Canada
[2]NOAA Earth System Research Laboratory, Chemical Sciences Division, 325 Broadway, Boulder CO 80305-3337, USA
[3]CEREVE, Université Paris Est, France
[4]Météo France, 1 Quai Branly, Paris 75005, France

Received: 5 November 2008 – Accepted: 8 January 2009 – Published: 4 February 2009

Correspondence to: S. Lovejoy (lovejoy@physics.mcgill.ca)

Published by Copernicus Publications on behalf of the European Geosciences Union.

Abstract

Due to unavoidable vertical fluctuations, the interpretation of atmospheric aircraft measurements requires a theory of turbulence. Until now virtually all the relevant theories have been isotropic. However almost all the available data on the vertical structure shows that it is scaling but with exponents different from the horizontal: the turbulence is anisotropic not isotropic. In this paper, we show how this can lead to spurious breaks in the scaling and to the spurious appearance of the vertical scaling exponent at large horizontal lags.

We demonstrate this using 16 legs of Gulfstream 4 tropospheric data following isobars each between 500 and 3200 km in length. First we show that the horizontal spectra of the aircraft altitude are nearly $k^{-5/3}$ (although smoothed by aircraft intertia at scales <3 km). In addition, we show that the altitude and pressure fluctuations along these fractal trajectories have a high degree of coherence with the measured wind (especially with its longitudinal component). There is also a strong phase relation between the altitude, pressure and wind fluctuations with all of these effects occurring over the entire range of scales so that the trajectories influence the wind measurements over large ranges of scale. In comparison, the temperature and humidity have no apparent scale breaks and the corresponding coherencies and phases are low reinforcing the hypothesis that it is the aircraft trajectory that is causally linked to the scale breaks in the wind measurements.

Using spectra and structure functions we then estimate the small and large scale exponents finding that they are close to the Kolmogorov values (5/3, 1/3) and the vertical values (2.4, 0.73) respectively (for the spectral and real space scaling exponents (β, H)) the latter are close to those estimated by drop sondes (2.4, 0.75) in the vertical direction. In addition, for each leg we estimate the energy flux, the sphero-scale and the critical transition scale. The latter varies quite widely from scales of kilometers to greater than several hundred kilometers. We theoretically explain this behaviour by considering the absolute slopes ($|\Delta z/\Delta x|$) of the aircraft as a function of lag Δx

ACPD

9, 3871–3920, 2009

and scale invariant lag $\Delta x/\Delta z^{1/H_z}$. Finally, we revisit four earlier aircraft campaigns including GASP and MOZAIC showing that they can be very easily explained by the proposed combination of altitude/wind and anisotropic but scaling turbulence.

1 Introduction

Aircraft are commonly used for high resolution studies of the dynamic and thermodynamic atmospheric variables and they are indispensable for understanding the statistical structure of the atmosphere in the horizontal direction. However, aircraft cannot fly in perfect horizontal straight lines, indeed recently (Lovejoy et al., 2004), it was shown that NASA's ER-2 stratospheric plane can have fractal trajectories. This means that the mean absolute slope increases at smaller and smaller scales being cut off only by the aircraft inertia. For the ER-2, the fractality of the trajectory could be traced to the plane's autopilot which kept the plane near a constant Mach number of 0.7, effectively enforcing long range correlations between the wind and the aircraft altitude.

The interpretation of such data requires assumptions about the turbulence and the mainstream turbulence theories are all isotropic. If they are correct, then neither the fractality nor a nonzero aircraft slope is of much consequence for the statistics of the fluctuations. However, if on the contrary the turbulence is anisotropic with different turbulent exponents in the horizontal and vertical directions then the interpretation may be different. Indeed such anisotropy is essentially the mainstream position of the experimentalists who have examined the vertical structure with "Jimspheres", radar, radiosondes or drop sondes (Adelfang, 1971; Endlich et al., 1969; Van Zandt, 1982; Fritts and Chou, 1987; Schertzer and Lovejoy, 1985b; Dewan and Good, 1986; Dewan, 1997; Lazarev et al., 1994; Tsuda et al., 1989; Gardner et al., 1995; Lovejoy et al., 2007, 2009a, see the review in Lovejoy et al., 2008a; Lilley et al., 2008; Radkevitch et al., 2008). For example, in the ER-2 case, the fractality of the trajectories leads to anomalous turbulent exponents while the existence of small nonzero slopes can lead to spurious transitions from the true horizontal exponents at small scales to the different

vertical exponent at large horizontal scales with the two separated by a spurious scale break. Lilley et al. (2008) re-examined two of the best known experimental estimates of horizontal wind spectra – the GASP and MOZAIC experiments (Nastrom and Gage, 1983, 1985; Nastrom et al., 1984; Gage and Nastrom 1986; Lindborg, 1999; Lindborg and Cho, 2001) – and showed that they can readily be explained – i.e. both their small and large scale regimes – by a single regime of wide range scaling 23/9 D anisotropic turbulence predicted by Schertzer and Lovejoy (1985b). Below (Sect. 5) we extend this re-evaluation of past measurement campaigns to include those of Gao and Meriwether (1998) (at 6 km) and Bacmeister et al. (1996) (stratosphere, 73 ER-2 flights) and show that they also readily fit into this framework.

Today, the use of state-of-the-art high resolution lidar (Lilley et al., 2004) and drop sondes (Lovejoy et al., 2007), has all but proved that the vertical is scaling but with nonstandard exponents. The latter paper is particularly relevant here because it used drop sondes dropped by a Gulfstream 4 aircraft during the month-long Pacific 2004 experiment whose simultaneous horizontal aircraft legs are analyzed below. Using 237 drop sondes at roughly 5 m resolution in the vertical, over 2700 scaling exponents for the horizontal wind were estimated and exponents near the classical values 1/3, 1 (the Kolmogorov law, the quasi-linear gravity wave theories, respectively, see below) were only obtained in half a dozen cases, with the mean slowly increasing from the (Bolgiano-Obukhov) value 3/5 near the surface to ≈0.75 at higher altitudes. Similarly, Lovejoy et al. (2009a) and Hovde et al. (2009) used the same sondes to determine the corresponding vertical exponents for temperature, pressure, humidity, potential temperature, equivalent potential temperature and air density showing that none had the exponents predicted by classical isotropic theories of turbulence.

If – as these studies suggest – the turbulence really is anisotropic with different horizontal and vertical exponents, then one must find new ways to interpret the aircraft measurements and to estimate the true statistics and horizontal exponents. While this was partially accomplished in the Lovejoy et al. (2004) study of the special ER-2 stratospheric aircraft, it is important to generalize the results and test them on the

somewhat different tropospheric aircraft data which attempt to follow isobars rather than isomachs (surfaces of constant Mach number).

This paper is structured as follows: in Sect. 2 we discuss the salient features of the data, in particular the slopes as functions of scale. In Sect. 3, we develop some theory to help interpret anisotropic turbulence measurements. In Sect. 4, we apply these to the data leg by leg and develop a new (Δx, Δz) analysis technique, in Sect. 5 we re-examine several past aircraft measurement campaigns and in Sect. 6 we conclude.

2 The data

2.1 The legs, slopes

The Pacific 2004 experiment is described in Hovde et al. (2009); it involved 10 aircraft flights over a roughly 2 week period over the northern Pacific each dropping 20–30 drop sondes. The plane flew along either the 162, 178, or 196 mb isobars, to within standard devations of ±0.11 mb (i.e. the pressure level was ≈constant to within ±0.068%), see Fig. 1a. Each had one or more constant straight and constant altitude legs more than four hundred kilometers long between 11.9, 13.7 km altitude (see Table 1 for details, see Fig. 1b for all the trajectories, and Fig. 1c for a blow-up showing the relation of the trajectories and the horizontal wind). The data were sampled every 1 s and the mean horizontal aircraft speed with respect to the ground was 280 m/s. In addition, we checked that the standard deviation of the distance covered on the ground between measurements was ±2% so that the horizontal velocity was nearly constant (in addition, using interpolation, we repeated the key analyses using the actual ground distance rather than the elapsed time and found only very small differences). Since the criterion for a "straight flat leg" was somewhat subjective, we used two different definitions; one which was not so conservative which used 16 straight and flat sections ("legs") constant to within ±450 m in the altitude and a smaller subset in all with altitudes to within ≈±150 m of a fixed level (see Fig. 1a and b for the distinction). In

ACPD
9, 3871–3920, 2009

the end, we did not find significantly different behaviour and the longer legs had the advantage of extending our analyses out to distances greater than 3200 km.

As can be seen, in spite of the attempt to use constant altitude legs, it was not quite constant because the pressure levels tended to rise or fall; we see that there is a mean slope of about 0.025 m/km; this was typical for an entire leg. However, this overall estimate is obviously a very crude characterization; indeed in Lovejoy et al. (2004) it was argued that the ER-2 stratospheric aircraft with special autopilot had a fractal trajectory:

$$S_z(\Delta x) = \langle |\Delta z(\Delta x)| \rangle \approx a \Delta x^{H_{tr}} \quad (1)$$

where a is a constant, $\Delta z(\Delta x)$ is the altitude change over a horizontal lag Δx, "$\langle\,\rangle$" indicates ensemble (statistical) averaging and $S_z(\Delta x)$ is the (first order) "structure function". For the ER-2 it was found that $H_{tr} \approx 0.55$ with an inner (smoothing) scale of about 3 km (as a consequence of aircraft inertia smoothing of the otherwise large slope variations) and an outer scale of the fractal regime at about 300 km due to the slow rise ($\approx$1 m/km) of the aircraft due to its fuel consumption; the ER-2 roughly followed isomachs rather than isobars. The fractal dimension of the trajectory is $D_{tr}=1+H_{tr}$; for the ER-2, $D_{tr} \approx 1.55$. In order to get a better idea of the typical slopes (s) as functions of scale, for each of the 16 short "legs" we estimated

$$\langle |s(\Delta x)| \rangle = \frac{\langle |\Delta z| \rangle}{\Delta x} = a \Delta x^{H_s}; \quad H_s = H_{tr} - 1 \quad (2)$$

these are shown in Fig. 2. From the figure we see that the steepest slopes are at the smallest scales and vary from about 2 to 5 m/km. It appears that for lags (Δx) greater than $\approx$3 km, the slopes follow a suggestive fractal Δx^{H_s} law with $H_s=-2/3$ which would result if the vertical displacement was proportional to the fluctuation in the horizontal wind speed, $\Delta z \propto \Delta v$ and if the latter follow a Kolmolgorov law in the horizontal $\langle |\Delta v(\Delta x)| \rangle \approx \varepsilon^{1/3} \Delta x^{1/3}$ (ε is the turbulent energy flux; we confirm this below). Since the lift and drag forces depend on the horizontal wind, a relation of the type $\Delta z \propto \Delta v$

ACPD
9, 3871–3920, 2009

for perturbations is not implausible. If this explanation is correct, the deviations for $\Delta x < 3$ km would be the result of aircraft inertia smoothing an otherwise even "rougher" trajectory. At large enough lags we see that each trajectory tends to a roughly constant mean absolute slope, although the lag and slope at which this occurs varies greatly from one trajectory to another from about 8 km to – in some cases – greater than the maximum i.e. >2000 km. These large Δx, "asymptotic" mean slopes vary from about 2.5 m/km to <0.25 m/km; these are roughly constant mean absolute slopes and reflect the large scale slopes of the isobars. The sequence of blowups in Fig. 1c shows that there is indeed some visual evidence for altitude/velocity correlations, particularly with the longitudinal component of the wind although it is subtle; see below. The situation is therefore somewhat different from that of the ER-2 trajectories, being controlled by the isobars rather than the isomachs.

2.2 Spectral analysis

To corroborate this interpretation further, we refer the reader to Fig. 3a which shows the spectra of the altitude z for each long leg. For clarity, the spectra are displaced in the vertical and have been normalized or "compensated" by dividing by the theoretical Kolmogorov spectrum ($k^{-5/3}$). Flat regions thus have spectra $\approx k^{-5/3}$. In addition, in order to show the behaviour more clearly – with the exception of the lowest 10 wavenumbers – we have averaged the spectrum over logarithmically spaced bins, 10 per order of magnitude. It can be seen that at $k > (3\,\mathrm{km})^{-1}$ that the spectrum is particularly steep corresponding to smooth behaviour (presumably due to the aircraft inertia as discussed above) whereas in the range roughly $(4\,\mathrm{km})^{-1}$ to $(100\,\mathrm{km})^{-1}$, the spectrum is $\approx k^{-5/3}$. At larger scales it rises steeply corresponding to the constant mean slope regime of Fig. 2.

In order to study the relation of this with the measured wind, it is useful to separate the latter into longitudinal and transverse components. This is done because on the one hand, even in isotropic turbulence the latter are in principle different, and on

the other hand because we expect that the longitudinal and transverse winds will have somewhat different effects – and hence relationships with the aircraft altitude (this was indeed found to be the case for the ER-2 measurements). In Fig. 3b and c we show the corresponding compensated spectra for each of the legs. By comparing Fig. 3a–c we are struck by the fact that they all share the same structure of three regimes at roughly $k=(3\,\mathrm{km})^{-1}$ and the second at much larger and highly variable scales (investigated in detail below). Since the breaks in the wind spectrum occur where the relation between the spectrum of aircraft altitude changes, this suggests that the vertical aircraft fluctuations strongly influence the measurements over wide ranges.

To clarify the picture, we averaged over the different legs, Fig. 3d. In order to have a uniformly sampled ensemble over the whole range of wavenumbers, we took 4000 point (≈1120 km) sections (this excluded leg 7, there were 24 segments from the remaining legs). We see that while the altitude spectrum has a rather accurate $k^{-5/3}$ regime over the range roughly $(3\,\mathrm{km})^{-1}$ to $\approx(200\,\mathrm{km})^{-1}$, that in fact the mean wind spectrum has two regimes, one for $k>(40\,\mathrm{km})^{-1}$ and a $k^{-2.4}$ regime for $k<(40\,\mathrm{km})^{-1}$. Finally, we also show the pressure spectrum finding that it has the same basic regimes as the altitude, and that for $k<\approx(100\,\mathrm{km})^{-1}$ is becomes much steeper indicating that the aircraft more accurately follows the isobars at these low wavenumbers than at higher ones. We argue below that most individual legs have these transitions although the transition point varies widely from leg to leg. Due to the clear dynamical relation between the wind field and the aircraft trajectory, we should not be surprised at finding a relation between the two. It is therefore of interest to compare this behaviour with that of the (relative) humidity and temperature neither of which are directly linked with the aircraft dynamics. Figure 3e shows the result for the averaged and compensated spectra (with the compensated versions of Fig. 3d for comparison). We see that both have excellent scaling, they are apparently unaffected by the trajectory fluctuations; we examine this more closely below.

ACPD
9, 3871–3920, 2009

2.3 Cospectral analysis

In order to further understand the statistical relation between the aircraft altitude and the wind statistics, we can calculate the spectral coherence. Consider the cross-spectrum S_{hg} and normalized (complex) cross-spectrum Cr_{hg} of two (1-D) functions h, g:

$$Cr_{hg} = \frac{S_{hg}}{(S_{gg}S_{hh})^{1/2}}; \quad S_{hg} = \langle \tilde{h}(k)\tilde{g}^*(k) \rangle \tag{3}$$

We can define the coherence C_{hg} and phase θ_{hg} as the modulus and phase:

$$Cr_{hg}(k) = C_{hg}(k)e^{i\theta_{hg}(k)} \tag{4}$$

(see e.g. Landahl and Mollo-Christensen, 1986). In Fig. 3f, averaging over all the legs, we show these for h=the altitude and g alternately taken as the longitudinal and transverse wind (left column) and h, g alternately taken as the pressure and (right column) longitudinal and transverse wind. Recall that due to the normalization $0 \leq C \leq 1$; C is a kind of wavenumber by wavenumber correlation coefficient with the important difference that it is positive definite. For identical functions, C=1 while for statistically independent functions, $C(k) \approx 1/\sqrt{n}$ where n is the number of independent samples. Here we considered the first 4000 points of each sufficiently long leg (so that n=24) hence the coherency for statistically independent wind and altitudes is $C(k) \approx 0.20$. In order to estimate the typical deviations around this mean value, we randomly paired altitudes of the nth leg with winds from a randomly chosen but different leg and calculated the resulting C (see Fig. 3f). We notice that the mean of this randomized coherency is near the theoretical value 0.20, with the "spread" decreasing with wavenumber (due to the fact that the number of wavenumber averaging bins increases with k).

The coherency is only the modulus; we therefore also considered the phases: $\theta = \theta_{zv}, \theta_{pv}$ (i.e. with h=z and p, respectively and g=v in Eq. (3), see Fig. 3g). With this choice, $\theta > 0$ indicates that the altitude (pressure) fluctuations lag behind the wind

ACPD
9, 3871–3920, 2009

fluctuations while $\theta<0$ indicates the converse. From Fig. 3f and g we consider the various regimes.

i) $k>(3\,\mathrm{km})^{-1}$. Starting the analysis at the small scales (large wavenumbers), we see that – as expected – due to the inertia of the aircraft which prevents it from rapidly responding to changes in wind, the coherency and phase with respect to the altitude is not statistically signficiant (left column). The situation is more interesting for the pressure (right column) where we see that the coherency of the transverse component with respect to the pressure is significant, and that the phase of the pressure lags behind the wind fluctuations. This is presumably the effect of fluctuations in the "dynamical pressure" caused by the wind changes.

ii) $(40\,\mathrm{km})^{-1}<k<(3\,\mathrm{km})^{-1}$. Moving to lower wavenumbers; we first remark that for the longitudinal component, there are apparent significant and even very strong coherencies and phase relations for essentially all the larger scales (although the statistics are poor beyond enough about $k<(500\,\mathrm{km})^{-1}$) with the relation between pressure and wind a bit stronger than that between altitude and wind. Over this range, the transverse component has only small coherencies and phase shifts, being significant only out to about $k<(40\,\mathrm{km})^{-1}$. When we consider the phases, we see that whereas the pressure continues to lag behind the wind ($\theta_{pv}<0$), the wind lags behind the altitude changes ($\theta_{zv}<0$). This could be a consequence of the autopilot (on a time scale of 10–100 s) adjusting the level due to the smaller scale turbulent trajectory fluctuations. Since the aircraft did not fly in any special direction with respect to the wind, the fact that there is such a difference between the longitudinal and transverse components is in itself strong evidence that the aircraft trajectory strongly affects the measurements.

iii) $k<(40\,\mathrm{km})^{-1}$–$(60\,\mathrm{km})^{-1}$. Finally, at the larger scales where the pressure and then the altitude no longer follow $k^{-5/3}$ spectra (Fig. 3e), we see that the phases of both the altitude and pressure with respect to the longitudinal component reverse sign. In this regime, the pressure leads the wind fluctuations while the altitude lags behind. This is presumably the regime in which the aircraft closely follows the isobars. From Fig. 3d and e we see that this is also the regime where the wind spectrum follows the $k^{-2.4}$ rather than $k^{-5/3}$ law; below we argue that it is this "imposed" vertical displacement that leads to the spurious appearance of the vertical exponent 2.4.

ACPD
9, 3871–3920, 2009

Large scale pressure/wind relations could arise naturally in the following way: along an isobar we have $dz = -\frac{\partial p}{\partial x} / \frac{\partial p}{\partial z} dx \approx dx \frac{\partial p}{\partial x} / (\rho g)$ where x is a coordinate parallel to the aircraft trajectory and we have used the hydrostatic approximation. If we also make the geostrophic approximation, $(\partial p/\partial x)/(\rho g) \approx -f v_y$, then we obtain the "geostrophic" slope: $s_{geo} = dz/dx \approx -f v_y/g$ where v_y is a transverse wind component and f is the Coriolis parameter.

Using data from the legs averaged at 40 km from the aircraft campaign we found that the actual slopes were only a little larger than these "geostrophic" slopes with mean ratio: 2.2±1.4. This gives evidence that the slopes of the isobars are indeed linked to the wind at these scales. This long-range meteorological effect could lead to large vertical fluctuations so that the wind fluctuations are mainly due to the vertical displacement of the aircraft. We could note that Fig. 2 already shows that the scale 40 km is only an average which hides very large leg to leg variations; this is further confirmed in Fig. 5 and in the sections below.

In Fig. 3c we see that $k \approx (40\,\text{km})^{-1}$ is indeed the critical scale for the (average) wind spectrum; for $k > (40\,\text{km})^{-1}$ the vertical fluctuations are not dominant and the spectrum is the (unbiased) horizontal Kolmolgorov value 5/3 where as for $k < (40\,\text{km})^{-1}$ the vertical fluctuations are sufficiently large so that the vertical exponent 2.4 is obtained.

As a final check, we also considered the temperature and humidity coherencies and phases (Fig. 3g). We see that over the regime $(40\,\text{km})^{-1} < k < (3\,\text{km})^{-1}$ there are only low coherencies and small phases for both, becoming insignificant for $k < (100\,\text{km})^{-1}$. The most statistically significant – the temperature phases – indicate that there is a lag with respect to the altitude, as expected if the altitude fluctuations were imposed by the autopilot. This overall weak link between the trajectory statistics and the temperature and humidity fluctuations is consistent with the excellent spectral scaling $k^{-\beta}$ (with $\beta = 2.13$, 2.10, respectively) over the entire range.

3 Understanding the effects of vertical aircraft motion on the velocity fluctuations

Let us consider a fairly general case of anisotropic but scaling turbulence so that the fluctuations in the horizontal velocity over a horizontal lag Δx and vertical lag Δz follow:

$$\Delta v = \varphi_h \Delta x^{H_h}; \quad \Delta v = \varphi_v \Delta z^{H_v} \tag{5}$$

where φ_h, φ_v are the turbulent fluxes dominant in the horizontal and vertical directions, respectively and H_h, H_v are the corresponding exponents. The (isotropic) Kolmogorov law is recovered with $\varphi_h=\varphi_v=\varepsilon^{1/3}$, $H_h=H_v=1/3$ where ε is the energy flux. In comparison, the original 23/9 D model of anisotropic turbulence (Schertzer and Lovejoy, 1985b) in which the horizontal is dominated by the energy flux (ε, $m^2\,s^{-3}$) and the vertical by buoyancy variance flux (ϕ $m^2\,s^{-5}$) is obtained with $\varphi_h=\varepsilon^{1/3}$, $\varphi_v=\phi^{1/5}$, $H_h=1/3$, $H_v=3/5$. Similarly, the popular quasi-linear gravity wave models (Dewan and Good, 1986; Dewan, 1997; Gardner, 1994; Gardner et al., 1993) typically take $\varphi_h=\varepsilon^{1/3}$, $\varphi_v=N$ (the Brunt Väisälä frequency; this is not a turbulent flux, a fact which is a serious weakness of that theory) so that $H_h=1/3$, $H_v=1$. In order to write these anisotropic models in a form valid for any vector in the vertical plane $\mathbf{\Delta r}=(\Delta x, \Delta z)$ we can use the formalism of Generalized Scale Invariance (Schertzer and Lovejoy, 1985a) and write:

$$\Delta v = \varphi_h \|\mathbf{\Delta r}\|^{H_h} \tag{6}$$

where the scale function (indicated by the double bars) replaces the usual vector norm appropriate for isotropic turbulence:

$$\|\mathbf{\Delta r}\| = l_s \left(\left(\frac{\Delta x}{l_s}\right)^2 + \left(\frac{\Delta z}{l_s}\right)^{2/H_z} \right)^{1/2}; \quad H_z = \frac{H_h}{H_v}; \quad l_s = \left(\frac{\varphi_h}{\varphi_v}\right)^{1/(H_v - H_h)} \tag{7}$$

where H_z is the exponent characterizing the degree of stratification ($H_z=1$ corresponds to isotropic 3-D turbulence, $H_z=0$ to isotropic 2-D turbulence) and l_s is the "sphero-scale" so-called because the structures are roundish at that scale. The scale function

need only satisfy a fairly general scale equation, so that the above form is only the simplest "canonical" scale function but is adequate for our purposes. It can be verified that if we successively take $\mathbf{\Delta r}=(\Delta x, 0)$ and $\mathbf{\Delta r}=(0, \Delta z)$ that we recover Eq. (5).

In such a turbulence, the volumes of structures (assumed isotropic in the horizontal) change with horizontal scale Δx as $\Delta x^{D_{el}}$ with $D_{el}=2+H_z$. The 23/9 D model derives its name because $H_z=(1/3)/(3/5)=5/9$; the quasi-linear gravity wave model has $H_z=1/3$ and therefore $D_{el}=7/3$ and we have noted that the classical 2-D and 3-D isotropic turbulences have $H_z=0$, 1 hence $D_{el}=2$, 3, respectively. The 23/9 D model of stratification was found to be obeyed quite precisely for passive scalar densities estimated by lidar (i.e. with the above scale function replacing the vector norm in the isotropic Corrsin-Obukhov law of passive scalar advection (Lilley et al., 2004, 2008); cf. $H_z=0.55\pm0.02$). Using drop sondes, it was also found that for the lower 2 km or so that the horizontal velocity (Lovejoy et al., 2007), also had $H_z\approx0.55$. However small but significant deviations were observed for higher altitudes so that $H_v\approx0.75$ and hence (assuming $H_h=1/3$) we infer that $H_z\approx0.44$. The origin of these deviations for the horizontal wind from the theoretical value is still not understood, they are especially puzzling since the theory holds quite accurately for passive scalars.

In order to understand the effect of the vertical trajectory variability on the horizontal wind statistics, consider a section with constant slope s:

$$\Delta v = \varphi_h l_s^{H_h} \left(\left(\frac{\Delta x}{l_s} \right)^2 + \left(\frac{s\Delta x}{l_s} \right)^{2/H_z} \right)^{H_h/2} \tag{8}$$

When considering the ER-2 trajectory, Lovejoy et al. (2004) pointed out that if s was constant, then there would exist a critical lag $\Delta x_c=l_s s^{1/(H_z-1)}$ such that for $\Delta x>\Delta x_c$, the second term would dominate the first and we would obtain:

$$\begin{aligned} \Delta v &= \varphi_h \Delta x^{H_h}; \quad \Delta x \ll \Delta x_c \\ \Delta v &= \varphi_v s^{H_v} \Delta x^{H_v}; \quad \Delta x \gg \Delta x_c \end{aligned} \tag{9}$$

We would therefore expect a spurious break in the horizontal scaling at Δx_c after which the aircraft would measure the vertical rather than horizontal statistics with exponent H_v rather than H_h. In the case of the ER-2, this was indeed the case for the longest lags dominated by the constant slope regime at around 300 km ($s \approx 1$ m/km caused by the aircraft losing weight due its fuel consumption). However, in his re-interpretation of the classical tropospheric turbulence campaigns using commercial airplanes (GASP, MOZAIC), Lilley et al. (2008) found that the horizontal wind spectra and structure functions, respectively could be explained if there was a transition from horizontal to vertical exponents at the somewhat smaller Δx_c's of around 30–50 km (i.e. about the same as the mean found here, Fig. 3c), see also the reanalyses in Sect. 5 of the spectra in Gao and Meriwether (1998), Bacmeister et al. (1994), Cho and Lindborg (2001), and Gage and Nastrom (1986). Unlike the ER-2 structure function, there was no indication of a significant intermediate fractal dominated regime in which the turbulent exponents are apparently biased by the long range correlation between the aircraft position/altitude and the turbulence it measures.

In order to understand the general effect of a fractal trajectory on the Δv statistics, we may consider a fractal trajectory obeying Eq. (1) with the simplifying "mean field" hypothesis that the mean result Eq. (1) can be used in place of Δz in Eq. (7) (this is equivalent to ignoring the correlations between the trajectory and the horizontal wind). It implies:

$$\langle |\Delta v| \rangle = \varphi_h l_s^{H_h} \left(\left(\frac{\Delta x}{l_s} \right)^2 + \left(\frac{a}{l_s} \right)^{2/H_z} (\Delta x^2)^{H_{tr}/H_z} \right)^{H_h/2} \quad (10)$$

we therefore see that there exists a critical trajectory exponent $H_{trc}=H_z$ such that for $H_{tr}>H_{trc}$ a spurious transition will occur at a critical Δx_c such that the second (vertical) term will dominate at $\Delta x>\Delta x_c$, while for small scales $\Delta x<\Delta x_c$ the first (horizontal) term will dominate. However, on the contrary for $H_{tr}<H_{trc}$ we find that the fractal nature of the trajectory will not lead to spurious scaling, it will not affect the horizontal exponent. We can now understand the key difference between our Gulfstream 4 data and

the ER-2. Over the range ≈3 km<Δx<300 km, the latter had an anomalous regime with $H_{tr}\approx 0.55\approx H_{trc}$ so that the above "mean field" type argument breaks down; we must carefully consider the (nontrivial) correlations between the wind and the trajectory, they can be important over a wide range. However, from Fig. 2, we can see that the Gulfstream 4 tropospheric isobaric trajectories analyzed here are different; they tend to involve abrupt transitions from $H_{tr}\approx 1/3$ to $H_{tr}\approx 1$ (i.e. $H_s\approx -2/3$ to $H_s\approx 0$) so that a spurious transition from horizontal to vertical exponents may or may not occur depending on the magnitude of the vertical fluctuations (a), the value of l_s (which depends on the relative magnitudes of the horizontal and vertical turbulent fluxes, Eq. 5), and the point at which the transition from $H_{tr}\approx 1/3$ to $H_{tr}\approx 1$ occurs.

Since turbulence is highly intermittent, in order to obtain robust estimates of exponents, experimentalists average their velocity fluctuations over as many lags as possible. Since $H_v > H_h$, it is enough that only some lags have a transition from horizontal to vertical behaviour for the spurious vertical scaling to dominate the ensemble statistics for large enough Δx. For each leg and for the averages over all the lags Δx, we therefore anticipate (c.f. Eq. 7) that:

$$\langle|\Delta v|\rangle = \left((A\Delta x)^2 + (B\Delta x)^{2H_v/H_h}\right)^{H_h/2} \quad (11)$$

for some empirically determined constants A, B. In order to test the hypothesis and to estimate the key exponents H_h, H_v, for each pair (H_h, H_v) we performed a regression on $\log_{10}\langle|\Delta v|\rangle$ to determine the constants A, B which minimized the root mean square residuals (error). In Fig. 4a we display a contour plot showing the behaviour of the error for components of the horizontal wind both transverse and longitudinal to the aircraft heading. There is a broad minimum; statistical analysis shows that minimum occurs at (H_h, H_v)=(0.26±0.07, 0.65±0.04), (0.27±0.13, 0.67±0.09) for the transverse and longitudinal components, respectively (the rms error in $\log_{10}\langle|\Delta v|\rangle$ at the minimum was about ±0.03 in both cases corresponding to deviations of only 100 ($10^{0.03}-1$) ≈±7% over 3–4 orders of magnitude in scale). As discussed earlier, the longitudinal component is more coherent with the altitude, this would explain its slightly larger error. Given the large

ACPD
9, 3871–3920, 2009

uncertainties, we can see that the H_h estimates are compatible with the Kolmogorov value H_h=1/3 while H_v is compatible with both the Bolgiano–Obukhov value 3/5 and the slightly larger value ≈0.75 observed from the (simultaneous) drop sondes in lower 1 km and the upper 12–13 km altitude range, respectively (corresponding to H_z=5/9, 0.44, respectively). Below, we shall see that not all legs show Δx^{Hv} regimes, and for some it is only visible for the largest Δx; this effect may lead to an underestimate of H_v.

If we assume that the Kolmogorov value H_h=1/3 is robust, we can fix it at that value and find the minimum error in estimates of as H_z=H_h/H_v is varied. Figure 4a shows the result; we see that the minima corresponds to the estimates: H_z≈0.46±0.05, 0.45±0.05 implying H_v=0.71±0.08, 0.73±0.08 for longitudinal and transverse components, respectively. We see that forcing H_h to take the theoretical value 1/3 leads to H_z and H_v values closer to those expected from the drop sondes (0.44, 0.75, respectively).

4 Leg by leg and (Δx, Δz) analyses

Now that we have reasonable estimates of the exponents – and in order to understand the results better – we can again consider the individual legs. Figure 5a and b shows the individual structure functions for each leg for the longitudinal and transverse components with regressions to the form Eq. (11) constrained to have H_h=1/3 and H_v=3/5 (thin line), H_v=3/4 (thick line). We see that the theoretical fits (with errors indicated in Fig. 4b ≈±0.04) are very good for both values of H_v with not much difference between them.

Using the regression coefficients A, B obtained with H_h=1/3, H_z=4/9, we can estimate the critical Δx_c at which the two terms in Eq. (11) are equal: Δx_c=$A^{H_z/(1-H_z)}$/$B^{1/(1-H_z)}$ (Table 1). We see that in two cases – leg 2 and leg 7 – that the $\Delta x^{1/3}$ law holds well over the entire leg so that no transition is observed (the corresponding entry is blank). Close examination of the corresponding slopes (Fig. 2) shows that these are cases with particularly long $s(\Delta x)$≈$\Delta x^{-2/3}$ regimes which – fol-

ACPD
9, 3871–3920, 2009

lowing our preceding analyses – favour the horizontal exponents (see also the spectra in Fig. 3). If in addition the l_s value is particularly large – and Radkevitch et al. (2008) shows empirically that it has huge fluctuations; the probability tail has a "fat" power law fall-off with exponent ≈1.33) – then there will be no transition over the observed range of lags Δx.

The direct regressions on the structure functions only give the coefficients A, B; these cannot be used directly to estimate l_s and ε. In addition, the analysis so far cannot rule out the possibility that the large scale turbulence is isotropic with genuine (rather than spurious) horizontal exponent $H_h \approx 0.7$–0.75 and with highly variable transition point. In this case for $\Delta x \gg \Delta z$, the Δz values will be statistically irrelevant for Δv; only the Δx values will be important. In order to rule out the latter possibility and to estimate l_s and ε we must use a different analysis technique. The key is to use the information of the Δv joint dependence on both Δx and Δz. Rewriting Eq. (7) we find:

$$\Delta = \overline{(\varepsilon^{1/3})}_\zeta (1 + l_s^{1-1/H_z} \zeta^{-1})^{1/3}; \quad \Delta = \frac{\overline{(|\Delta v(\Delta x, \Delta z)|)}_\zeta}{\Delta x^{1/3}}; \quad \zeta = \frac{\Delta x}{\Delta z^{1/H_z}} \tag{12}$$

Where we use the average over constant ζ (denoted by the overbar and subscript) of $\varepsilon^{1/3}$ and the normalized gradient Δ. ζ is the "scale invariant lag" since under generalized scale changes $\mathbf{T}_\lambda = \lambda^{-\mathbf{G}}$ (where G is the generator of the scale changing group – in this case $\mathbf{G} = ((1, 0), (0, H_z))$) if we start with a unit vector $\mathbf{\Delta r}_1 = (\Delta x_1, \Delta z_1)$ with associated $\zeta_1 = \Delta x_1 \Delta z_1^{-1/H_z}$, the scale changing operator $\mathbf{T}_\lambda$ yields the λ times smaller reduced vector $\mathbf{\Delta r}_\lambda = \mathbf{T}_\lambda \mathbf{\Delta r}_1$ but with $\zeta_\lambda = (\lambda \Delta x_1)(\lambda^{H_z} \Delta z_1)^{-1/H_z} = \zeta_1$, i.e. unchanged. In order to improve the statistics, we used all the $n(n-1)/2$ pairs of measurements for each n point long leg, hence yielding robust behaviour and parameter estimates. Figure 6 shows the leg by leg result (on the short legs) along with the optimum regression to determine ε, l_s (the former is simply the large ζ asymptote); these are given in Table 1. The figure shows that the theoretical form fits very well over an impressive 8 orders of magnitude in ζ. The main deviations are at the small ζ values, but this reflects that the fact that

the small ζ values are not numerous so that the statistics are not well estimated; they are from rare large vertical "jumps" over short distances. We note that there are no signs of deviations from the theoretical behaviour at large ζ corresponding to long and flat displacements. In other words, we can rule out a large scale transition to isotropic $H_h=H_v\approx 0.7$ turbulence since the longest, flattest displacements have $H_h=1/3$.

Aside from the strong support that the figure gives to our conclusions about the effect of anisotropic turbulence, we can also note that it confirms that legs 2, 7 have nearly perfect $\Delta x^{1/3}$ behaviours over the entire range. We can also note from the table that the values of ε are highly variable (as expected) but the geometric mean ($\approx 4\times 10^{-4}\,\mathrm{m^2\,s^{-3}}$) is not so far from the "typical values" 10^{-3}–$10^{-4}\,\mathrm{m^2\,s^{-3}}$ measured elsewhere.

We see that the estimates of l_s are in the range 3 cm to about 70 cm which is exactly the range of the direct estimates from lidar in Lilley et al. (2004) (9 cross-sections of passive scalar lidar backscatter ratios, each with $2<l_s<80$ cm) and a little larger than the estimate from the mean ER-2 data ($l_s\approx 4$ cm). Recall that since $H_v>H_h$, l_s is the scale at which structures begin to become flattened in the horizontal. Using this value of l_s, we can calculate an "effective slope" s_{eff} which is the constant slope that would explain the transition at Δx_c from horizontal to vertical scaling statistics (see Table 1):

$$s_{\mathrm{eff}} = \frac{B l_s}{(A l_s)^{1/H_z}} \tag{13}$$

We see that the values are quite large – in the range 7–25 m/km; this shows that the behaviour cannot be understood in terms of a roughly constant s over an entire leg; the wind/altitude coherency is more subtle than that.

We might mention at this point that here we have considered that the scaling exponents H_h, H_v apply to the behaviour along orthogonal axes defined by the local gravity field. However, this may be only an approximation: theoretically the axes need not be exactly orthogonal (corresponding to non diagonal generators of the anisotropy). This might arise as a consequence of some strong shear for example. The physically relevant s would be then slope with respect to these axes and not with the local gravity

ACPD
9, 3871–3920, 2009

field.

5 Comparison with other aircraft studies

We have argued that aircraft measurements of wind have systematically ignored the effect of fluctuations/variations in the altitude of the measurements and that as a consequence, at large enough scales the measured wind fluctuations spuriously have vertical scaling exponents rather than the true horizontal exponents (for the spectra, ≈2.4 and ≈5/3, respectively). Although we mentioned that this has been verified in Lilley et al. (2008) on two of the main atmospheric campaigns (GASP and MOZAIC), we would like to revisit these quickly along with two others showing that they are very close to those here (Fig. 3d) and can be convincingly explained by the combination of vertical aircraft fluctuations coupled with anisotropic but scaling turbulence.

The GASP experiment was perhaps the most influential experiment to date on the horizontal spectrum, being generally interpreted as lending support to 2-D turbulence at large scales. However, this interpretation is fraught with difficulties since the claimed 2-D k^{-3} behaviour would only be in the narrow range between about 500 and 3000 km; see Fig. 7a. Restricting ourselves to isotropic turbulences this would imply that the 3-D $k^{-5/3}$ range extends way beyond the atmospheric scale height 10 km requiring that the 3-D turbulence be "squeezed to become nearly two-dimensional" (Högstrom et al., 1999) with an energy flux source localized in scale somewhere around 500 km (Lilley, 1983); Högstrom et al. (1999) proposes that this source might be convection). Additionally, this model would require an enstrophy source at around 3000 km – given in this classical picture possibly by baroclinic instabilities.

While this classical interpretation is forced – involving as it does two ad hoc sources and an unclear "squeezing" mechanism – as shown by the added thick lines (slope −2.4), the spectra are in fact very simple to explain with the anisotropic turbulence mechanism described here, indeed the transition point (10 and 100 km for meridional and zonal components, respectively) is quite close to the mean transition point found

ACPD
9, 3871–3920, 2009

here (Fig. 3d, 40 km). However, the spectrum shown in Fig. 7a is actually a composite of spectra with legs in three different length categories. When focusing on the larger scales it is thus more pertinent to focus on the longest leg category only; those longer than 4800 km. When this is done (Fig. 7b), our reinterpretation is made all the more convincing since the large scale is seen to be nearly exactly of the predicted $k^{-2.4}$ form, with no plausible k^{-3} regime whatsoever.

The GASP experiment involved commercial airliners flying along isobars near the top of the troposphere. It is therefore of interest to compare this with the (Gao and Meriwether, 1998) analysis of 11 legs of the scientific Electra aircraft which also flew along isobars (see Fig. 7c) but at ≈6 km. Concentrating on their spectra of horizontal wind, we find once again that exponents of 2.4 and 5/3 with a transition at about 10 km explain the data very easily; the authors' overall regression estimate 1.98 (over the range 1–100 km) being a rough average of the two. Also, their regression giving a 3.18 exponent is only over the range 100–330 km and is not compelling. While our interpretation is fairly straightforward, the authors offer no explanation for their value 1.98.

In the introduction, we mentioned that the most recent major campaign (>7600 flights) was the MOZAIC campaign which – like the GASP experiment – also involved commercial aircraft flying along isobars (between 9.4 and 11.8 km). Figure 7d shows the second order structure function from Cho and Lindborg (2001). The spectral exponent $\beta=1+\zeta(2)$ where $\zeta(2)$ is the second order structure function exponent so that the vertical exponent $\beta=2.4$ corresponds to $\zeta(2)=1.4$. In the figure we see that our picture of a transition from horizontal exponent 2/3 to vertical exponent 1.4 accurately accounts for the data over all the range (except for the extreme factor of 2–3 where the structure function levels off, a typical symptom of poor statistics) with the transition occurring at about 50 km i.e. about the same scale as in Fig. 3c. Also shown is a reference line r^2 which is the basic prediction of 2-D turbulence. Given the divergence of their curve from the r^2 line, it is surprising that Cho and Lindborg (2001) nevertheless claimed support for a 2-D isotropic turbulence regime. They did this by adding in a log

ACPD
9, 3871–3920, 2009

correction. While such a correction is theoretically predicted in pure 2-D (Kraichnan) theory, it is normally considered a small effect and ignored. However Cho and Lindborg's claim to be able to save the 2-D theory by using log corrections was seriously undermined in the Lilley et al. (2008) reanalysis. They showed that the price paid in using log corrected r^2 law to explain a (near) $r^{1.4}$ law over an order of magnitude in scale is that the corrections must be so large as to imply impossible negative variances for scales ≈4000 km and larger.

In the introduction, we mentioned the stratospheric analyses Lovejoy et al. (2004) obtained from ER-2 aircraft following isomachs rather than isobars which found fractal trajectories with somewhat higher fractal dimensions (≈1.55) than those found here (≈1.33). These results are quite similar to those of Bacmeister et al. (1996) (Fig. 7e). Again, we see that over the analyzed range 0.4–102 km the data follows the slopes 5/3 and 2.4 quite well. In Bacmeister et al. (1996) exponents were estimated scale by scale and leg by leg so that histograms were built up. While at the small scales, the mean exponent is near ≈5/3, at the larger scales, as predicted, this value increases to about 2.5.

6 Conclusions

6.1 Discussion

In this paper, we examine in more detail the characteristics of 16 horizontal tropospheric aircraft legs with an aim to systematically determine the consequences of the anisotropic turbulence on the vertically fluctuating trajectories. By calculating the mean absolute slopes as functions of scale, we discovered that for $\Delta x > 3$ km there is a significant intermediate fractal regime with $\Delta z \approx \Delta x^{H_{tr}}$, with $H_{tr} \approx 1/3$ followed (usually) at large Δx by a transition to a regime with a mean constant slope, i.e. $H_{tr}=1$. At scales $\Delta x < 3$ km the slopes were lower than one would expect from an extrapolation from the fractal regime; presumably a consequence of the aircraft inertia. We argued that

while the fractal regime was presumably dominated by turbulence, that the highly variable transition point from $H_{tr} \approx 1/3$ to $H_{tr} \approx 1$ depended on the level of turbulence, the slopes of the isobars and perhaps even the pilot and autopilot. By considering spectra and coherencies between the altitude and the wind and altitude (z) and pressure (p) measurements we showed that for most of the range of scales >3 km, that statistically significant coherencies and phase relations exist between z and the longitudinal wind and even stronger coherencies and phase relations between p and the longitudinal wind (and to much lesser degrees with the transverse wind). Since the aircraft did not fly in directions with special orientations the mere fact that the behaviour of the transverse and longitudinal wind were different in this regard supports the hypothesis that it is an artifact of the altitude/wind correlations. By examining the corresponding cross-spectral phases, we were able to show that these were also statistically significant over most of the range, with the wind fluctuations leading those of the altitude at the small (<3 km) aircraft inertial scales after which the altitude fluctuations lead the wind fluctuations up to ≈40 km followed by a further reversal corresponding precisely to the $k^{-2.4}$ range of the average spectrum, this time presumably due to meteorological correlations between the slopes of the isobars and the wind. The relation between the pressure and the wind was even stronger and clearer: at scales less than ≈40 km the pressure fluctuations lagged behind the wind fluctuations (especially the longitudinal wind) with a complete reversal at larger scales with the wind lagging behind the pressure. The intimate relation between altitude, pressure and wind statistics over even larger distances makes our reinterpretation compelling. In future, robotic aircraft ought to be fitted out so that they record the inputs and outputs to the autopilot. That way the aircraft motion relative to the atmosphere could, at least in principle, be solved as a problem in Newtonian physics and the relation of aircraft altitude to the meteorology could further clarified.

Using a "mean field" approximation (which ignores the correlation between the vertical fluctuations and the wind), we showed that for the trajectory fluctuations $\Delta z(\Delta x) \approx \Delta x^{H_{tr}}$, there is a critical exponent H_z such that if $H_{tr} < H_z$ then the turbulence

ACPD
9, 3871–3920, 2009

will not affect the scaling of the horizontal wind, i.e. we continue to find $\Delta v \approx \Delta x^{H_h}$, while for $H_{tr} > H_z$ there will be a spurious break with the vertical exponent dominating for large Δx where $\Delta v \approx \Delta x^{H_v}$. The prediction that at there will be two scaling regimes separated by a break was directly tested using the ensemble statistics; it was found to hold with high accuracy with $H_h \approx 0.27 \pm 0.10$, $H_v \approx 0.66 \pm 0.07$. Due to the large uncertainties, we took this as confirmation that the Kolmogorov value $H_h \approx 1/3$ was correct, and we noted that the vertical value is somewhat biased to small values since most but not all trajectories had a Δx^{H_v} dominated regime. Fixing $H_h = 1/3$ lead to the refined estimate $H_z = H_h/H_v = 0.455 \pm 0.05$ implying $H_v \approx 0.73$ which is very close to the drop sonde estimate 0.75 for the 12–13 km level.

While these ensemble analyses supported the basic picture, new insight was obtained by looking at the legs individually. In particular, it was found that the transition point Δx_c separating the Δx^{H_h} and Δx^{H_v} regimes was itself highly variable – in two cases being larger than the length of the trajectory (at least several hundreds of kilometers) while in some instances it was smaller, of the order of 10 km. This high variability was itself predicted on the basis of the observed slope statistics, the high intermittency of the turbulence and the consequence of following isobars rather than constant altitudes. It goes a long way towards explaining the plethora of horizontal scale breaks reported in the literature.

As a final test, we considered the predictions of the theory for the scale invariant lags $\zeta = \Delta x / \Delta z^{1/H_z}$; this method takes into account the detailed vector fluctuation $\mathbf{\Delta r} = (\Delta x, \Delta z)$, i.e. the joint horizontal and vertical displacements of the aircraft. In this case the theoretical predictions were verified over 8 orders of magnitude in ζ. It enabled us to rule out the possibility that there is a genuine large scale isotropic turbulent regime with exponent $H_v = H_h \approx 0.7$–0.75, since the longest flattest displacements followed $H_h = 1/3$ very accurately. In addition the method allowed us to estimate the energy flux ε and the sphero-scale l_s. Both values were found to be quite plausible given the published determinations in other experiments, notably the sphero-scale – the scale at which typical structures are roundish (they become increasingly flat at

larger scales) – was found to be in the range 20 cm to 2 m, very close to the ER-2 estimate (4 cm) and the lidar estimate (10–80 cm). As a general matter this scale invariant lag technique could profitably be used to remove the effect of the vertical fluctuations for analyzing other atmospheric fields. This will be developed further elsewhere.

6.2 Implications for our understanding of the atmosphere

The last thirty years has seen such a vast improvement in our ability to measure, analyze and model the atmosphere that at first sight it is incredible that there is still no consensus about its most basic statistical characteristics including the way that wind fluctuations vary with scale. Closer consideration however shows that no matter how precise or plentiful our measurements may be, that they nonetheless require theories, models and assumptions for their interpretation. The use of aircraft data in understanding the structure of the atmosphere provides a sobering illustration of this dialectic.

It now seems that the interpretations have invariably been naïve: they have either simply ignored the vertical motion of the aircraft or have assumed that the turbulence is isotropic so that the vertical fluctuations do not strongly affect the statistics. When the analyses show breaks in the horizontal scaling (as they invariably do), rather than question the isotropy assumption and reinterpret the data, scientists tend to casually invoke the existence of two or more horizontal scaling regimes. The break between them is typically attributed to a transition from small scale three-dimensional isotropic turbulence to large scale two-dimensional isotropic turbulence and this, even if the break point varies considerably from experiment to experiment, and even if it is much bigger than the atmospheric scale height of 10 km. However – as pointed out by Schertzer and Lovejoy (1985b) the very existence of such a "dimensional transition" (once called a "meso-scale gap", (Van der Hoven, 1957)) is itself only a theoretical consequence of the a priori assumption that turbulence must be isotropic! If the turbulence is anisotropic but scaling, then structures may simply become flatter and flatter at larger and larger scales in a power law manner and such a transition is unnecessary. This is indeed the strong conclusion of a recent massive planetary scale study of short and long wave

radiances (Lovejoy et al., 2009b). In this way, we see that the entire mainstream view of the atmosphere has fundamentally been coloured by the assumption of isotropic turbulence.

Cracks in this isotropic edifice started to appear in the 1980s when evidence started to mount that the key horizontal wind field has vertical statistics – including the scaling exponents – that were very different from those in the horizontal, suggesting that isotropic turbulence might be irrelevant to atmospheric dynamics. Incredibly, a recent literature review (Lilley et al., 2008) failed to find a single experimental study of the vertical which claimed evidence for the Kolmogorov scaling exponent H_v=1/3 – at any location or at any scale. On the contrary for twenty years, the debate among experimentalists on the vertical statistics has been between the values 3/5 (Bolgiano–Obukhov), 1 (quasi-linear gravity waves), and now with the more precise drop – sonde estimates, H_v=0.60–0.75 (low to high altitudes, still not well understood (Lovejoy et al., 2007). See Tuck (2008) for a discussion of anisotropic turbulence in the context of fluid mechanics.

The implications of these anisotropic scalings have not yet been translated into a proper understanding of the influence of vertical aircraft fluctuations nor into the interpretation of their measurements, nor into their significance for our overall understanding of the atmosphere. However, given persistent central role played by isotropic theories of turbulence, the ramifications make take many years to fully discern.

Acknowledgements. We acknowledge NOAA funding of the Winter Storms 2004 mission. This research was performed purely for scientific purposes, it did not enjoy any specific funding.

References

Adelfang, S. I.: On the relation between wind shears over various intervals, J. Atmos. Sci., 10, 138, 1971.

Bacmeister, J. T., Eckermann, S. D., Newman, P. A., Lait, L., Chan, K. R., Loewenstein, M., Proffitt, M. H., and Gary, B. L.: Stratospheric horizontal wavenumber spectra of winds, pot-

netial temperature, and atmospheric tracers observed by high-altitude aircraft, J. Geophys. Res., 101, 9441–9470, 1996.
Cho, J. and Lindborg, E.: Horizontal velocity structure functions in the upper troposphere and lower stratosphere i: Observations, J. Geophys. Res., 106, 10223–10232, 2001.
Dewan, E. and Good, R.: Saturation and the "universal" spectrum vertical profiles of horizontal scalar winds in the stratosphere, J. Geophys. Res., 91, 2742–2752, 1986.
Dewan, E.: Saturated-cascade similtude theory of gravity wave sepctra, J. Geophys. Res., 102, 29799–29817, 1997.
Endlich, R. M., Singleton, R. C., and Kaufman, J. W.: Spectral analyes of detailed vertical wind profiles, J. Atmos. Sci., 26, 1030–1041, 1969.
Fritts, D. and Chou, H.: An investigation of the vertical wavenumber and frequency spectra of gravity wave motions in the lower stratosphere, J. Atmos. Sci., 44, 3611–3623, 1987.
Gage, K. S. and Nastrom, G. D.: Theoretical Interpretation of atmospheric wavenumber spectra of wind and temperature observed by commercial aircraft during GASP, J. Atmos. Sci., 43, 729–740, 1986.
Gao, X. and Meriwether, J. W.: Mesoscale spectral analysis of in situ horizontal and vertical wind measurements at 6 km, J. Geophys. Res., 103, 6397–6404, 1998.
Gardner, C.: Diffusive filtering theory of gravity wave spectra in the atmosphere, J. Geophys. Res., 99, 20601–20605, 1994.
Gardner, C., Tao, X., and Papen, G.: Simultaneous lidar observations of vertical wind, tmeprea-ture and density profiles in the upper atmsophere: evidence of nonseperability of atmo-spheric perturbation spectra., Geophys. Res. Lett., 22, 2877–2888, 1995.
Gardner, C. S., Hostetler, C. A., and Franke, S. J.: Gravity Waqve models for the horizontal wave number spectra of atmospheric velocity and density flucutations, J. Geophys. Res., 98, 1035–1049, 1993.
Hovde, S. J., Tuck, A. F., Lovejoy, S., and Schertzer, D.: Vertical Scaling of the Atmosphere: Dropsondes from 13 km to the Surface, Q. J. Roy. Meteorol. Soc., submitted, 2009.
Landahl, M. T. and Mollo-Christensen, E.: Turbulence and Random Processes in Fluid Me-chanics, Cambridge University press, Cambridge, 154 pp., 1986.
Lazarev, A., Schertzer, D., Lovejoy, S., and Chigirinskaya, Y.: Unified multifractal atmospheric dynamics tested in the tropics: part II, vertical scaling and generalized scale invariance, Nonlin. Processes Geophys., 1, 115–123, 1994, http://www.nonlin-processes-geophys.net/1/115/1994/.

Lilley, M., Lovejoy, S., Strawbridge, K. B., and Schertzer, D.: 23/9 dimensional anisotropic scaling of passive admixtures using lidar aerosol data, Phys. Rev. E, 70, 036307-036301-036307, 2004.
Lilley, M., Lovejoy, S., Schertzer, D., Strawbridge, K. B., and Radkevitch, A.: Scaling turbulent atmospheric stratification, Part II: empirical study of the the stratification of the intermittency, Q. J. Roy. Meteorol. Soc., 134, 301–315, doi:10.1002/qj.202, 2008.
Lindborg, E.: Can the atmospheric kinetic energy spectrum be explained by two-dimensional turbulence?, J. Fluid Mech., 388, 259–288, 1999.
Lindborg, E. and Cho, J.: Horizontal velocity structure functions in the upper troposphere and lower stratosphere ii. Theoretical considerations, J. Geophys. Res., 106, 10233–10241, 2001.
Lovejoy, S., Schertzer, D., and Tuck, A. F.: Fractal aircraft trajectories and nonclassical turbulent exponents, Phys. Rev. E, 70, 036306-036301-036305, 2004.
Lovejoy, S., Tuck, A. F., Hovde, S. J., and Schertzer, D.: Is isotropic turbulence relevant in the atmosphere?, Geophys. Res. Lett., 34, L14802, doi:10.1029/2007GL029359, 2007.
Lovejoy, S., Schertzer, D., Lilley, M., Strawbridge, K. B., and Radkevitch, A.: Scaling turbulent atmospheric stratification, Part I: turbulence and waves, Q. J. Roy. Meteorol. Soc., 134, 277–300, doi:10.1002/qj.1201, 2008.
Lovejoy, S., Tuck, A. F., Hovde, S. J., and Schertzer, D.: The vertical cascade structure of the atmosphere and multifractal drop sonde outages, J., Geophys. Res. in press, 2009a.
Lovejoy, S., Schertzer, D., Allaire, V., Bourgeois, T., King, S., Pinel, J., and Stolle, J.: Atmospheric complexity or scale by scale simplicity?, Geophys. Res. Lett., 36, L01801, doi:10.1029/2008GL035863, 2009b.
Nastrom, G. D. and Gage, K. S.: A first look at wave number spectra from GASP data, Tellus, 35, 383–397, 1983.
Nastrom, G. D., Gage, K. S., and Jasperson, W. H.: Kinetic energy spectrum of large and meso-scale atmospheric processes, Nature, 310, 36–38, 1984.
Nastrom, G. D. and Gage, K. S.: A climatology of atmospheric wavenumber spectra of wind and temperature by commercial aircraft, J. Atmos. Sci., 42, 950–960, 1985.
Radkevitch, A., Lovejoy, S., Strawbridge, K. B., Schertzer, D., and Lilley, M.: Scaling turbulent atmospheric stratification, Part III: empIrical study of Space-time stratification of passive scalars using lidar data, Q. J. Roy. Meteorol. Soc., 134, 316–335, doi:10.1002/qj.1203, 2008.
Schertzer, D. and Lovejoy, S.: Generalised scale invariance in turbulent phenomena, Physic-

ochem. Hydrodyn., 6, 623–635, 1985a.
Schertzer, D. and Lovejoy, S.: The dimension and intermittency of atmospheric dynamics, in: Turbulent Shear Flow 4, edited by: Launder, B., Springer-Verlag, New York, pp. 7–33, 1985b.
Tsuda, T., Inoue, T., Fritts, D., VanZandt, T., Kato, S., Sato, T., and Fukao, S.: MST radar observations of a saturated gravity wave spectrum, J. Atmos. Sci., 46, 2440–2458, 1989.
Tuck, A.: ATMOSPHERIC TURBULENCE: A Molecular Dynamics Perspective, Oxford University Press, 2008.
Van der Hoven, I.: Power spectrum of horizontal wind speed in the frequency range from .0007 to 900 cycles per hour, J. Meteorol., 14, 160–164, 1957.
Van Zandt, T. E.: A universal spectrum of buoyancy waves in the atmosphere, Geophys. Res. Lett., 9, 575–578, 1982.

Table 1. This compares the various characteristics of the 16 nearly straight, flat legs considered in this paper. The column Max(Δz) is the difference in altitude between the highest and lowest points on the leg, Δx_c is the critical scale beyond which the vertical exponent dominates the horizontal (Eq. 9) (here estimated as the geometric mean between the longitudinal and transverse values using the regression on Eq. 11). For legs 2 and 7, the transition was not attained over the entire leg so that only a lower bound is given. We also give the energy flux ε and the sphero-scale l_s are determined by Eq. (12), and the effective dimensionless slope s_{eff} from Eq. (13).

Leg no.	Short Length (km)	Short Max(Δz) (m)	Long Length (km)	Long Max(Δz) (m)	Δx_c (km)	s_{eff}	$\varepsilon \times 10^4$ ($m^2 s^{-3}$)	l_s (m)
1	2100	72	2100	72	12.4	0.02	0.3	0.04
2	1248	83	1248	83	>1200	–	0.2	–
3	1136	44	2496	69	84	0.01	40.	0.14
4	1988	285	3348	737	108	0.008	0.2	0.05
5	1136	267	2044	631	12.8	0.02	0.4	0.07
6	908	89	1476	260	7.6	0.02	0.2	0.03
7	568	19	568	19	>400	–	0.3	–
8	1136	84	1588	206	30.4	0.01	1.2	0.08
9	2924	100	2924	100	384	0.008	30.	0.09
10	1276	32	2272	172	40	0.02	40.	0.25
11	568	229	2980	899	100	0.01	0.4	0.10
12	568	203	3292	883	260	0.007	0.4	0.13
13	1532	308	1532	308	52	0.02	0.2	0.60
14	1704	204	3408	597	64	0.01	0.5	0.09
15	1648	57	2780	191	3.6	0.03	5.	0.11
16	852	46	1844	178	48	0.01	2.0	0.05

ACPD
9, 3871–3920, 2009

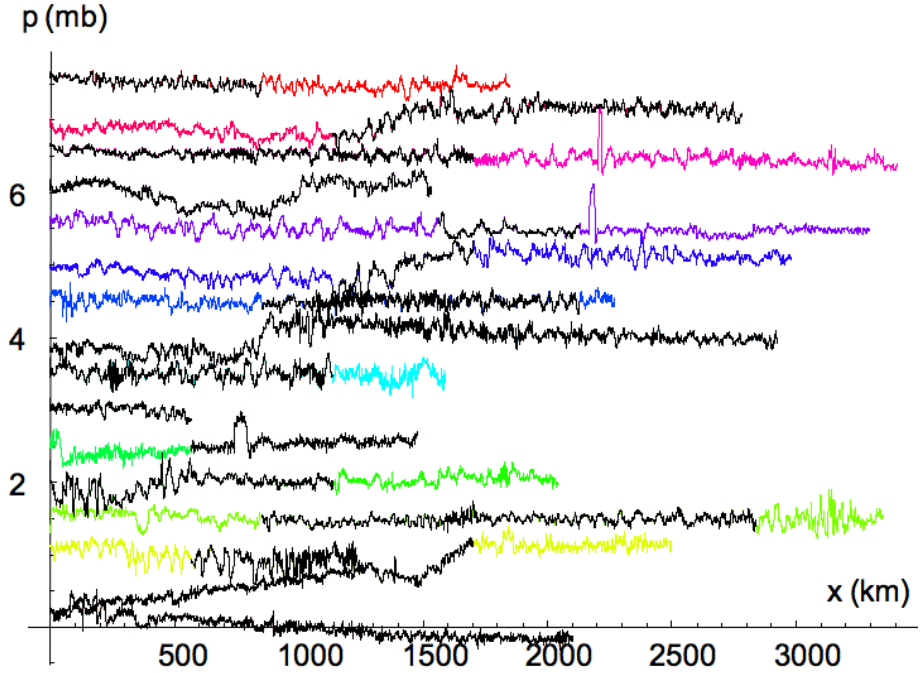

Fig. 1a. The pressure as a function of horizontal position for legs analyzed in this paper. For clarity, the deviations from the minimum pressure are displaced in the vertical by 0.5 mb per curve. The black sections indicate the short legs. The absolute pressures were all between 162 and 196 mb.

ACPD
9, 3871–3920, 2009

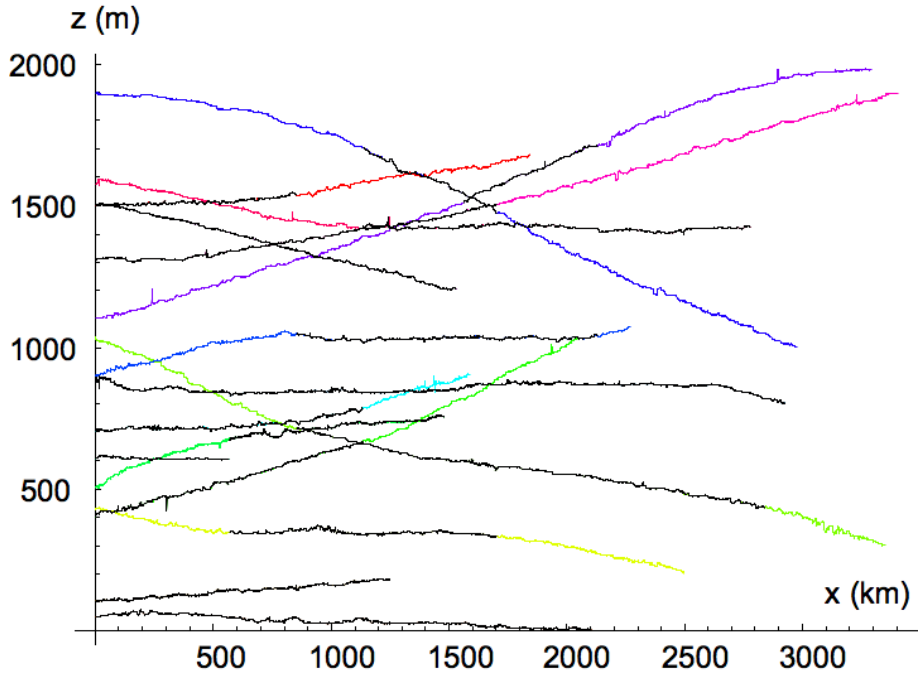

Fig. 1b. The altitude as a function of horizontal position for legs analyzed in this paper. For clarity, the deviations from the minimum altitude are displaced in the vertical by 100 m per curve. The black sections indicate the short legs.

ACPD
9, 3871–3920, 2009

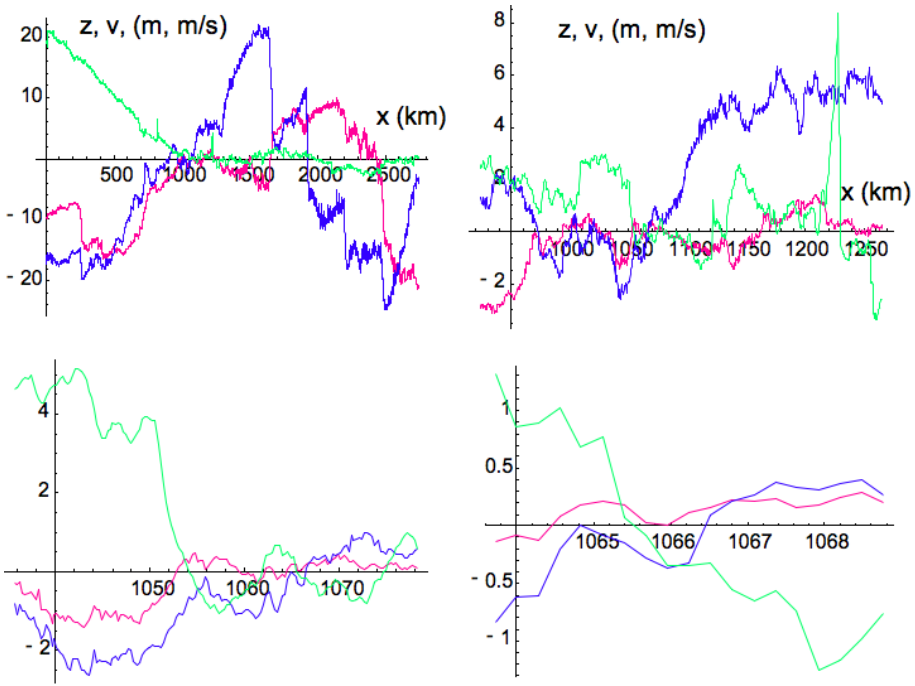

Fig. 1c. This shows four blow ups of factor 8 starting at the upper left, then upper right, lower left, lower right. Green shows the deviations of z from the 12 700 m of the altitude of the aircraft, (in m) but divided by 8, 4, 2, 1, respectively. The red shows the variation in the longitudinal component of the horizontal velocity (in m/s, deviations from 24.5 m/s), and the blue is the transverse component (in m/s, deviations from 1.2 m/s). This is for leg 15, but was typical.

ACPD
9, 3871–3920, 2009

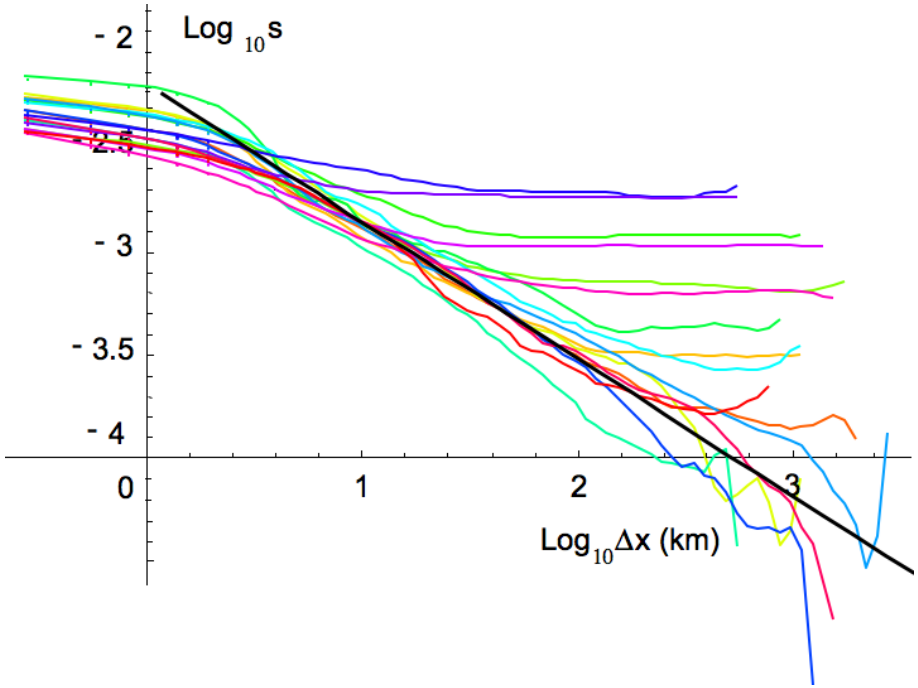

Fig. 2. This shows the mean dimensionless slope as a function of scale for each of the 16 legs. For reference, we show in black the line $s \approx \Delta x^{-2/3}$ corresponding to $H_{tr}=1/3$. The structure function S was estimated by averaging over all disjoint lags. Since the number of such lags decreases with increasing Δx, the statistics are not so good for the large Δx.

ACPD
9, 3871–3920, 2009

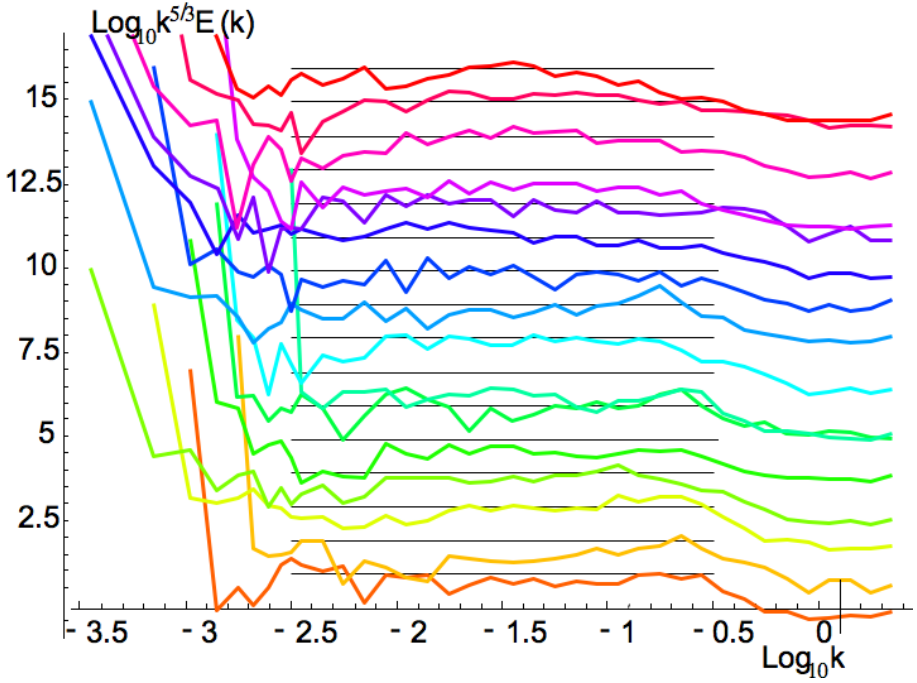

Fig. 3a. This shows the horizontal spectrum of the altitude for each of the legs (1–16 bottom to top, each displaced by an order of magnitude for clarity). In order to see the trends more clearly, for $k>10$, the spectra were averaged over 10 bins per order of magnitude in wavenumber. The spectra are compensated by dividing by $k^{-5/3}$ so that the flat regions follow a Kolmogorov $k^{-5/3}$ law corresponding to a $\Delta x^{-2/3}$ law for the slope in Fig. 2. The Kolmogorov law is found to hold well except at the lowest wavenumbers. The units of each wavenumber are (km^{-1}) the highest wavenumber corresponds to 2 samples, i.e. 2 s or 560 m.

ACPD
9, 3871–3920, 2009

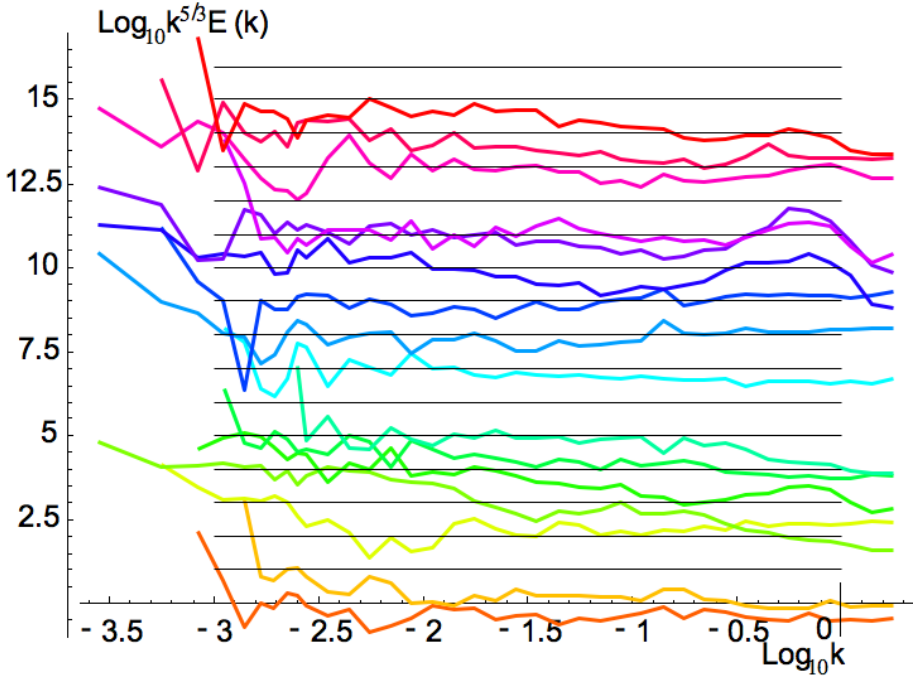

Fig. 3b. The same as Fig. 3a except for the longitudinal component of the wind. The low wavenumber rise seen in most of these corresponds to a roughly $k^{-2.5}$ spectrum; the spectral counterpart of H_h=0.75 behaviour (ignoring small intermittency corrections).

ACPD
9, 3871–3920, 2009

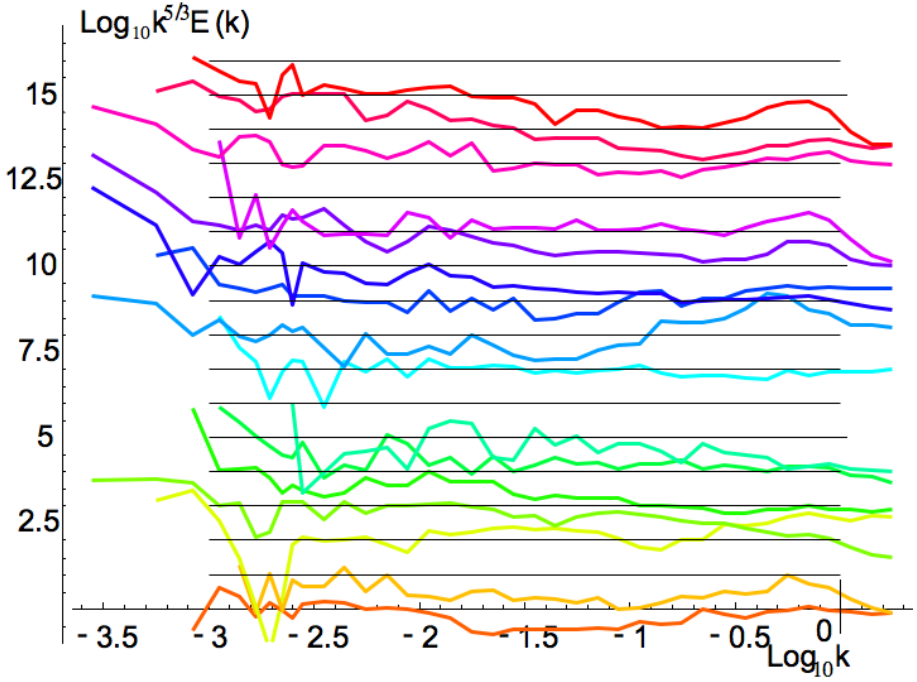

Fig. 3c. The same as Fig. 3b except for the transverse component of the wind.

ACPD
9, 3871–3920, 2009

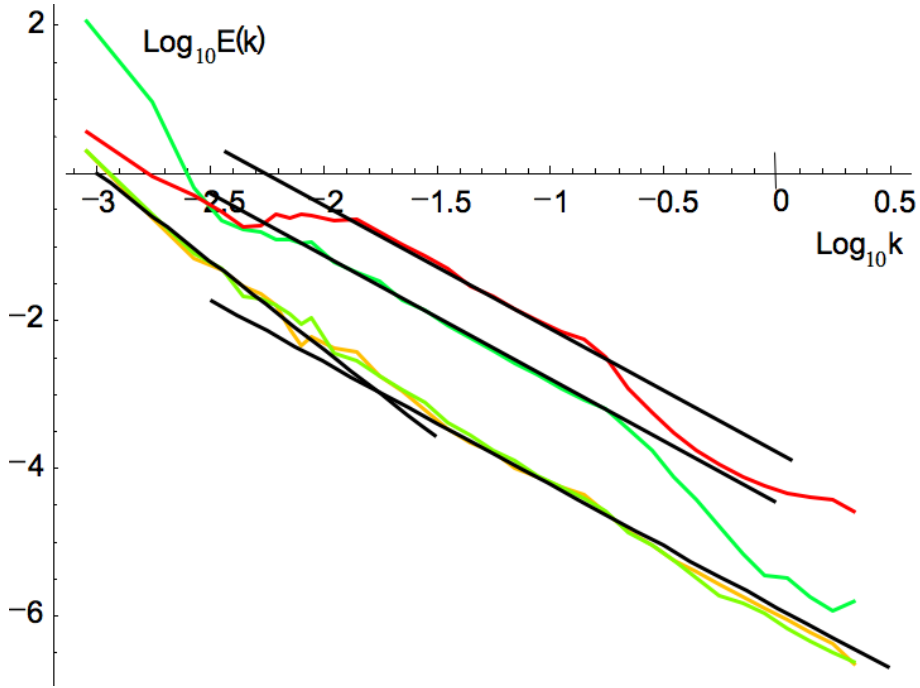

Fig. 3d. The first 4000 points (1120 km) of the legs (excluding number 7 which was too short) were used to estimate these ensemble spectra which were averaged over all the legs and over, ten wavenumber bins per order of magnitude (k in units of km^{-1}). The pressure (red, top) and altitude (green, second from top), the transverse (orange, bottom) and longitudinal (green, bottom) winds are shown with reference lines indicating the theoretical vertical spectrum ($k^{-2.4}$) and the theoretical horizontal spectrum $k^{-5/3}$. The average transition wavenumber is about (30 km)$^{-1}$.

ACPD
9, 3871–3920, 2009

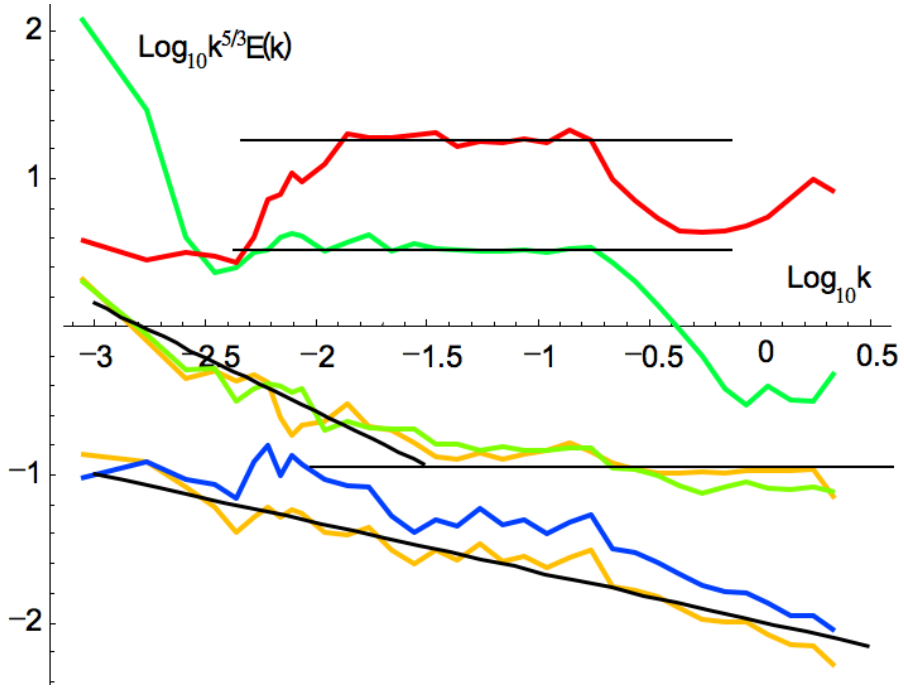

Fig. 3e. Top to bottom: this shows the compensated pressure (red), altitude (green), longitudinal, (green, third from top), transverse, (orange, fourth from top) humidity (blue, second from bottom) and temperature (orange, bottom). Reference slopes correspond to $k^{-5/3}$ (flat), $k^{-2.4}$ and k^{-2}. The spectra are for 24 legs each 1120 km long, averaged over 10 per order of magnitude.

ACPD
9, 3871–3920, 2009

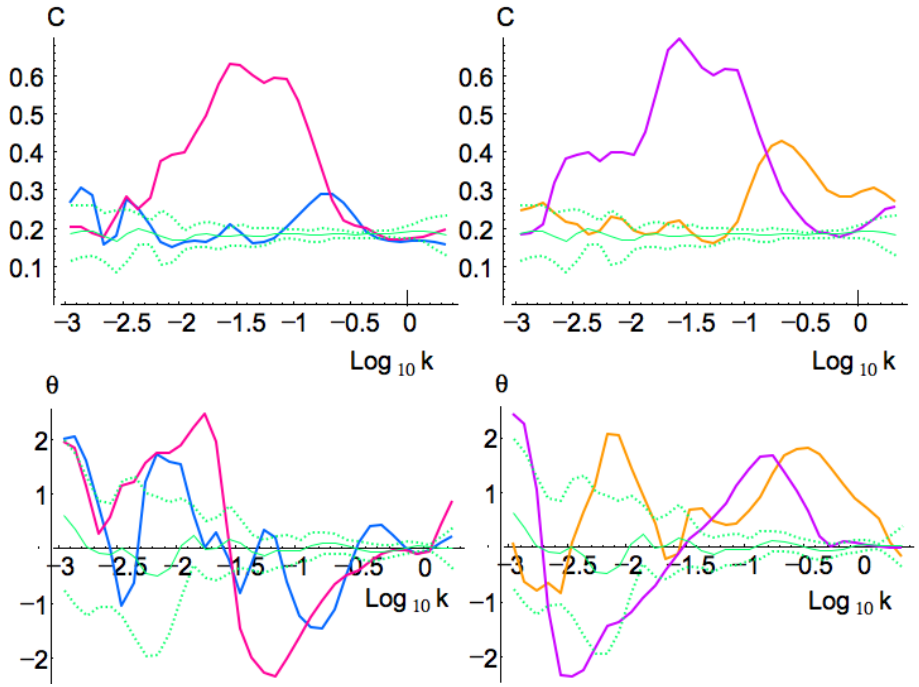

Fig. 3f. This shows the coherency (top row) and phases (bottom row) of the cross spectra of altitude (left column) and pressure (right column) with transverse wind (blue altitude, left; orange, pressure, right), longitudinal wind (red, altitude, left; purple, pressure, right), units km^{-1}. The coherency and phases were averaged over logarithmically spaced bins, 10 per order of magnitude (except for the lowest 10 wavenumbers). Green shows the mean (thick) and standard deviation (dashed) of the randomized coherencies and phases as discussed in the text. Phases and coherencies are only statistically significant when outside the corresponding ranges.

ACPD
9, 3871–3920, 2009

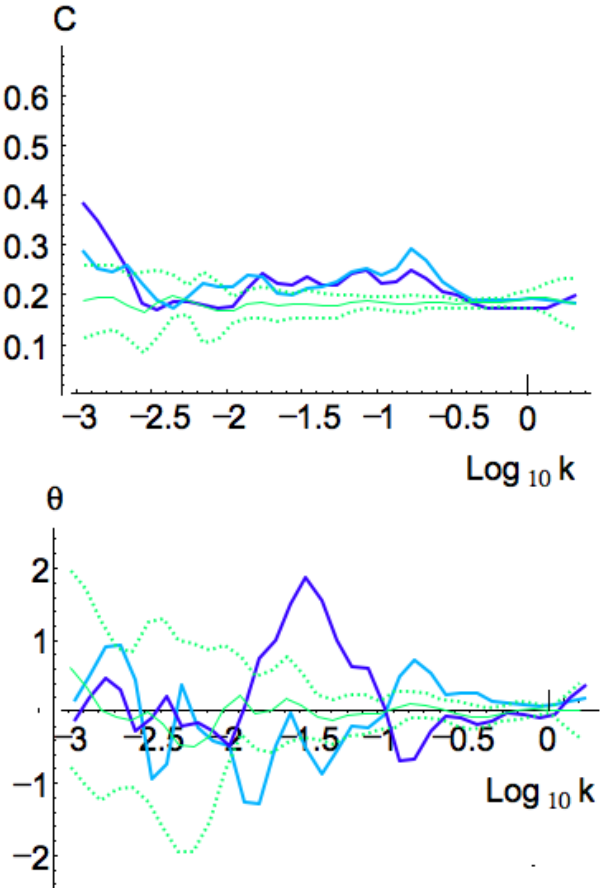

Fig. 3g. Similar to Fig. 3f, this shows the coherencies (top) and the phases (bottom) of the cross spectra of altitude with temperature (blue), humidity (cyan), k in units km^{-1}.

ACPD
9, 3871–3920, 2009

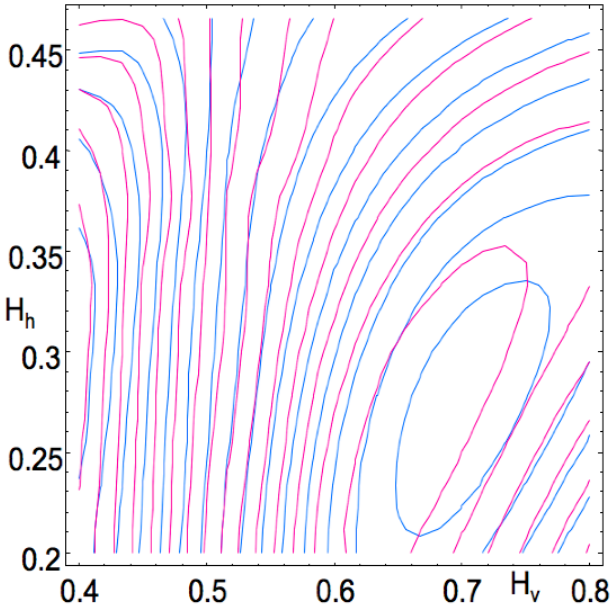

Fig. 4a. A contour plot of the rms errors in estimating $\log_{10}\langle|\Delta v|\rangle$ using the formula Eq. (11). The longitudinal and transverse components of the horizontal winds are shown in pink, blue, respectively. The centre of the diagram corresponds to the theoretical values $(H_h, H_v)=(1/3, 3/5)$. The minima are at $(H_h, H_v)=(0.26\pm0.07, 0.65\pm0.04)$, $(0.27\pm0.13, 0.67\pm0.09)$ for the transverse and longitudinal components, respectively.

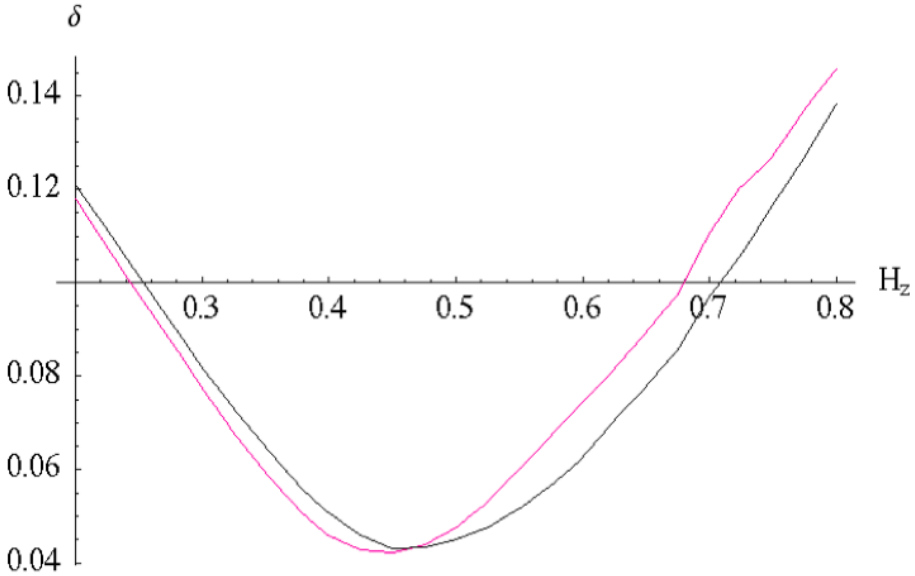

Fig. 4b. The rms error in estimating for longitudinal (black) and transverse (red) components, respectively obtained by fixing H_h=1/3. The minima correspond to the estimates: H_z≈0.46±0.05, 0.45±0.05 for longitudinal and transverse components, respectively.

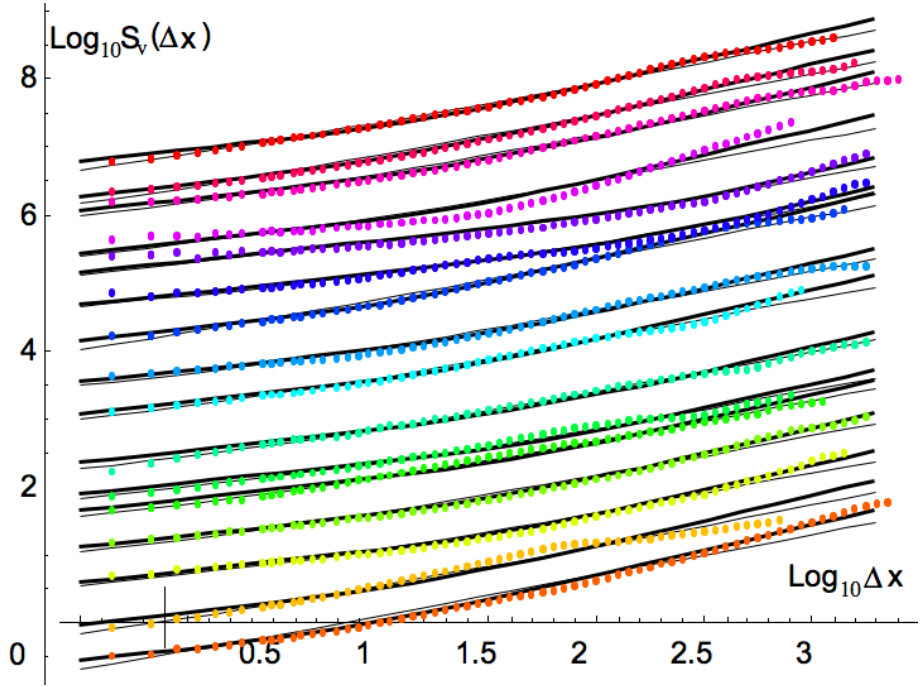

Fig. 5a. This shows the first order structure function for the longitudinal component of the horizontal wind for each of the 16 legs, each displaced by 0.5 in vertical for clarity. Δx is the horizontal distance in km. The thin line is the regression to the form Eq. (11) with H_z=4/9 while the thick line has H_z=5/9.

ACPD
9, 3871–3920, 2009

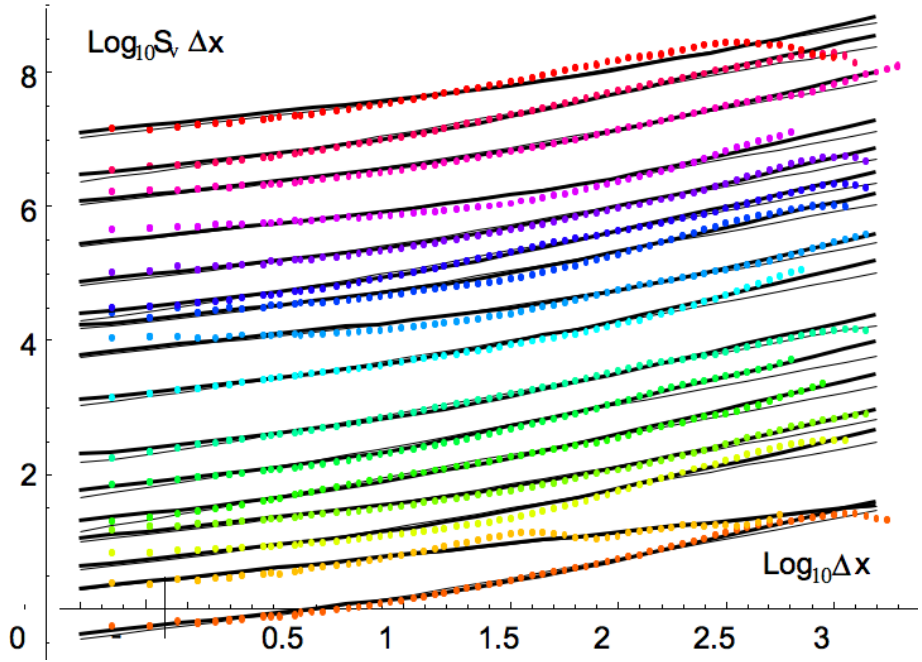

Fig. 5b. Same as Fig. 5a except for the transverse component.

ACPD
9, 3871–3920, 2009

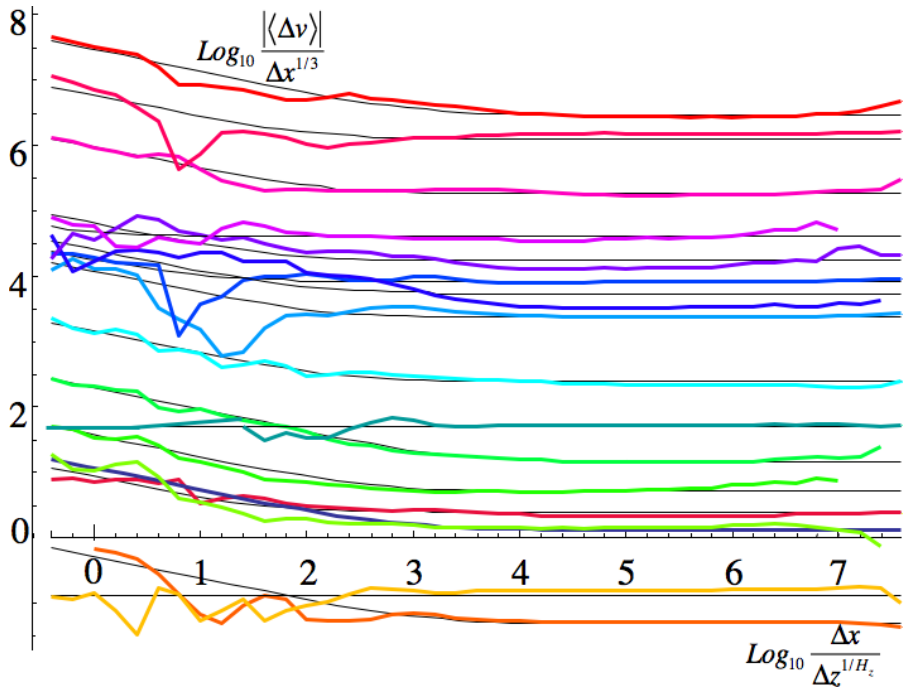

Fig. 6. This shows the normalized mean velocity difference Δ as a function of the scale invariant lag $\zeta = \Delta x / \Delta z^{1/H_z}$ with $H_z = 4/9$. The legs are shown displaced vertically for clarity (legs 1–16, bottom to top). The statistics of long flat lags are to the right, short, highly sloped lags to the left. The black lines give regressions to the form Eq. (12). Using $H_z = 5/9$ doesn't change the appearance very much.

ACPD
9, 3871–3920, 2009

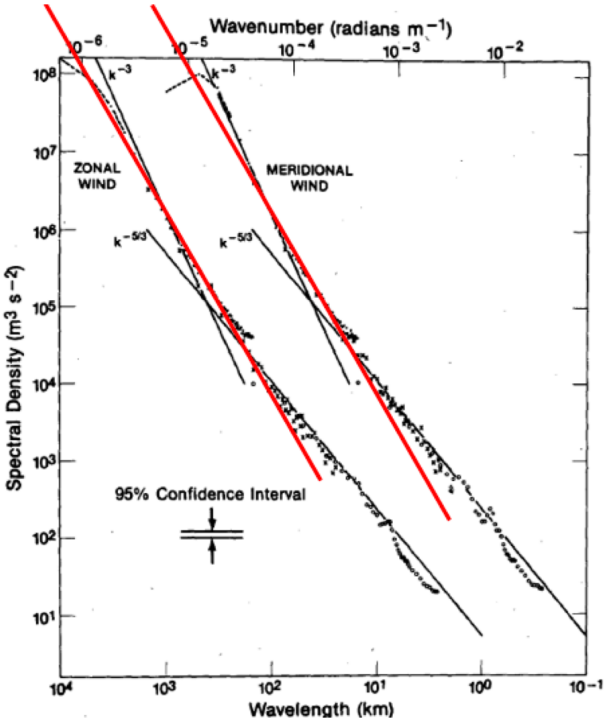

Fig. 7a. Key GASP results adapted from Gage and Nastrom (1986) with data broken into three groups depending on trajectory length (different symbols). It can be seen that the thick added reference lines with vertical exponent 2.4 fit very well from roughly 10 and 100 km on up (meridional and zonal components).

ACPD
9, 3871–3920, 2009

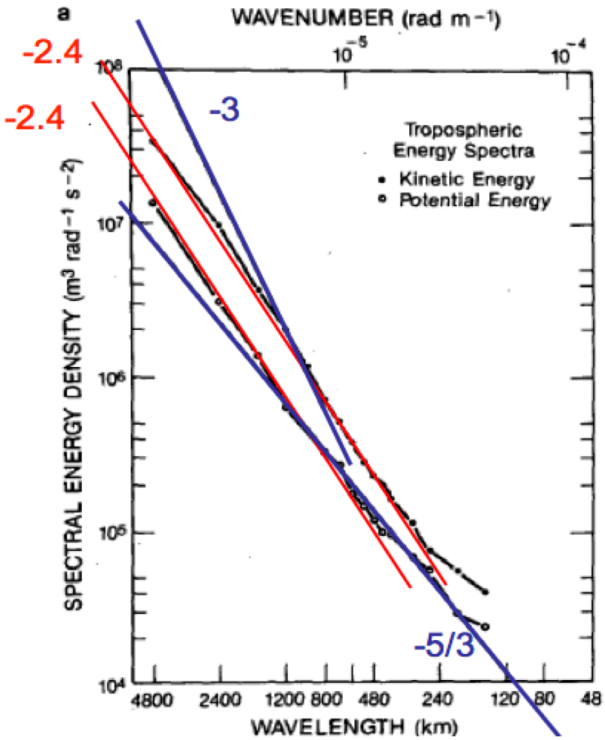

Fig. 7b. Adapted from Gage and Nastrom (1986) with the reference lines corresponding to the horizontal and vertical behaviour discussed in the text (exponents 5/3, 2.4, i.e. ignoring intermittency corrections corresponding to H_h=1/3, H_v=0.7 as well as the 2-D isotropic turbulence slope −3). This figure shows the spectra only for the particularly long legs (at least 4800 km long).

ACPD
9, 3871–3920, 2009

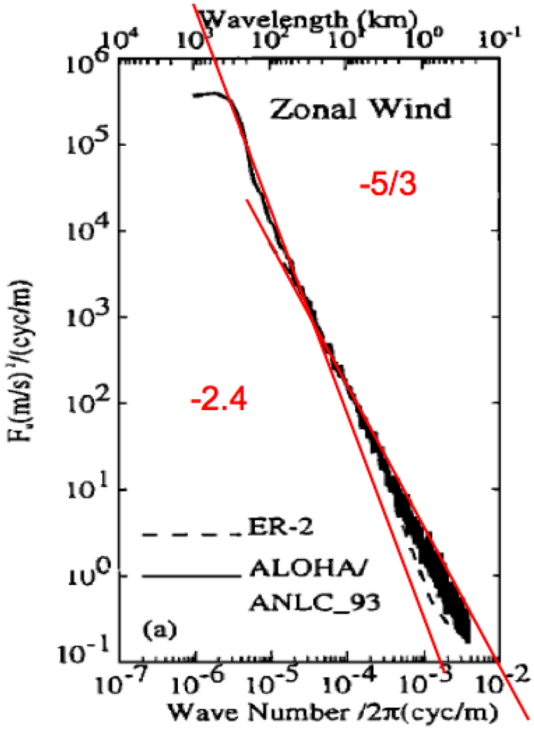

Fig. 7c. The averaged spectra adapted from Gao and Meriwether (1998) at 6 km altitude with the horizontal and vertical exponents discussed here indicated as reference lines.

ACPD
9, 3871–3920, 2009

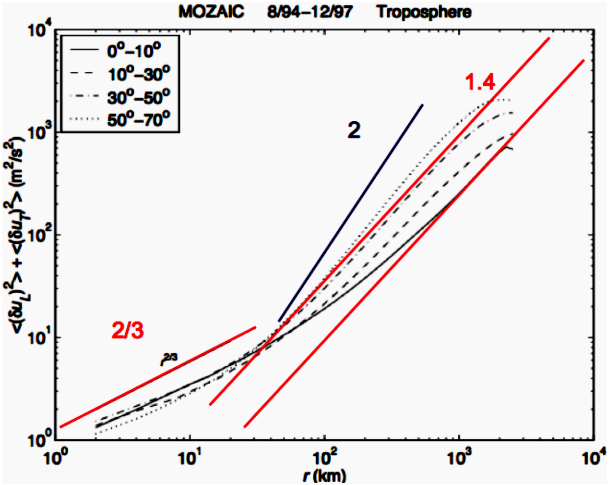

Fig. 7d. Adapted from Lindborg and Cho (2001): second order structure functions of the horizontal wind (sum of longitudinal and transverse components). Since the spectrum is (essentially) the fourier transform of the structure functions, the spectral behaviour $k^{-\beta}$ corresponds to $r^{(\beta-1)}$, hence the corresponding reference lines.

ACPD
9, 3871–3920, 2009

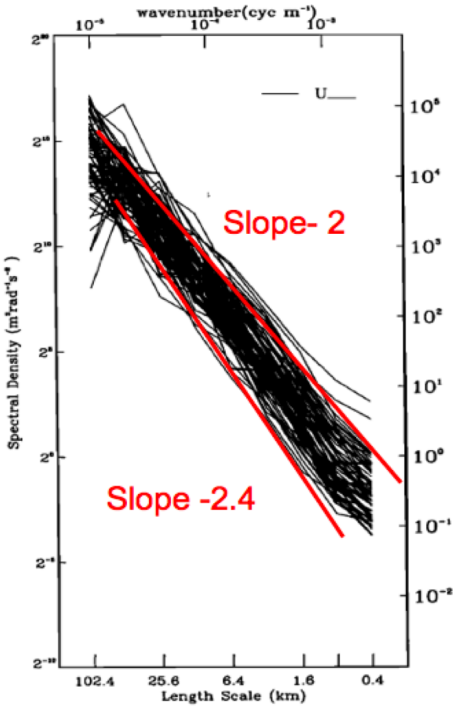

Fig. 7e. Stratospheric ER-2 spectra adapted from Bacmeister et al. (1996), Fig. 5. This is a random subset of 1024 s long legs, again with reference slopes added.

ACPD
9, 3871–3920, 2009